Performance of Numerical Basis Set DFT for Aluminum Clusters

David J. Henry, Adrian Varano, and Irene Yarovsky*

Applied Sciences, RMIT University, GPO Box 2476V, Victoria, 3001, Australia

Received: March 19, 2008; Revised Manuscript Received: June 10, 2008

We have investigated and compared the ability of numerical and Gaussian-type basis sets combined with density functional theory (DFT) to accurately describe the geometries, binding energies, and electronic properties of aluminum clusters, $Al_{12}XH_n$ (X = Al, Si; n = 0, 1, 2). DFT results are compared against high-level benchmark calculations and experimental data where available. Properties compared include geometries, binding energies, ionization potentials, electron affinities, and HOMO−LUMO gaps. Generally, the PBE functional with the double numerical basis set with polarization (DNP) performs very well against experiment and the analytical basis sets for considerably less computational expense.

1. Introduction

There has been considerable interest in the structure and reactivity of metal clusters and nanostructures for use as building blocks of new materials, particularly those with closed electronic shells due to their high stability.[1−4] Experimental studies of the ionization potentials,[5,6] electron affinities (or electron detachment energies of Al_n^-),[7−11] static polarizabilities,[12] dissociations,[13−15] and reactivities [5,16,17] of aluminum clusters have identified Al_{13} as a particularly stable structure which has also been supported by a range of theoretical studies.[18−30] This stability has been attributed to the fact that Al_{13} has 39 valence electrons and therefore is only one electron short of being closed shell in the jellium model.[31] In fact the Al_{13}^- anion and $Al_{12}Si$ clusters, which have 40 valence electrons and are therefore closed shell, are even more stable than Al_{13}.[7−11,32−40] A number of experimental[41] and theoretical[42−49] studies have shown that a hydrogen atom can also stabilize the Al_{13} cluster by providing the necessary additional electron to form a closed-shell aggregate.

Density functional theory (DFT) has been applied widely to the study of metal clusters and nanostructures with varying degrees of success. Clearly the choice of functional plays an important role in the accuracy of a given result. A recent study by Han et al.[47] investigated the performance of a small number of functionals and analytical basis sets for the description of the geometric and electronic properties of Al_{13} and $Al_{13}H$. However, numerical basis sets can offer some significant advantages over analytical basis sets, particularly in terms of computational efficiency.

As with Gaussian-type basis sets, numerical basis functions are expressed as the product of a radial function and a spherical harmonic. The numerical part is obtained by numerically solving the atomic DFT equations, which along with the $-(\nabla^2/2)$ terms (required for the evaluation of the kinetic energy) are represented as a set of cubic spline coefficients, thereby making them piecewise analytic. This representation makes the generation of analytic energy gradients much easier. Furthermore, Delley reports[50] that molecules can be dissociated exactly into their constituent atoms (within the DFT context), thereby minimizing or even eliminating basis set superposition error (BSSE). These sets are computationally efficient, a feature which arises from the confinement of the atomic basis sets (from which the numerical basis set is constructed) within a cutoff value r_c. Strict localization of the basis set within r_c is ensured via a soft-confinement potential, and the derivatives at r_c are continuous. The basis sets implemented in DMol[3] were constructed specifically for use in DFT calculations.

Systematic studies concerning the performance of numerical basis sets within DFT are scarce. It is intended that the present study will complement and extend the work of Han et al.[47] by studying the performance of a numerical and two analytical basis sets with the PBE and PW91 functionals against high-level theoretical and experimental values, for the description of Al_{13} and $Al_{12}Si$, their monocations, monoanions, and simple hydrides of these clusters.

Another feature we are interested in investigating is the effect of electronic occupation scheme on calculated properties of aluminum clusters. Generally, quantum chemistry packages use by default a Fermi occupation of orbitals, appropriate for application to covalently bonded systems; however, computational codes designed for application to metallic systems often provide a smearing or thermal occupation option to aid with convergence. The DMol[3] program enables the application of either standard Fermi occupations or, alternatively, a thermal occupation procedure, which uses a finite-temperature Fermi function to compute fractional occupation of orbitals, generally deemed suitable for metallic systems, and is sometimes necessary to achieve convergence of the density. In this study we present results for $Al_{12}XH_n$ (X = Al, Si; n = 0, 1, 2) clusters obtained with several density functionals with analytical basis sets and Fermi occupations, and with a numerical basis set using both Fermi occupations and thermal occupations. Results are compared with CCSD and G3(MP2)-RAD values and available experimental and theoretical values from the literature.

2. Theoretical Methods

Standard density functional theory and ab initio calculations were performed using the DMol[3],[50] Gaussian 03,[51] and MOLPRO[52] computer programs. Geometries for Al_{13}, $Al_{12}Si$, and their respective monocations and monoanions were calculated with the PBE[53] and PW91[54] functionals using the DNP, 6-31G(d,p), and 6-311G(d,p) basis sets, and at the CCSD/6-31G(d,p) level, which provides a benchmark level for geometries in the absence of experimental data. Calculations with the

* To whom correspondence should be addressed. E-mail: Irene.yarovsky@rmit.edu.au.

10.1021/jp802389b CCC: $40.75
Published on Web 09/10/2008

6-31G(d,p) and 6-311G(d,p) basis sets were performed in Gaussian, while calculations in DMol^3 were performed with the double numerical polarized (DNP) basis set. Each of these basis sets include a *d*-type polarization function on heavy atoms and a *p*-type polarization function on hydrogen. The DNP basis set is comparable in size to the Gaussian-type 6-31G(d,p) basis set. It was previously shown that an all-electron basis set with the addition of *d* functions is essential for a proper description of high-valence Al atoms.[55]

Binding energies and adiabatic ionization potentials (IPs) and electron affinities (EAs) were evaluated at each level used for geometry optimization and compared with values obtained with a modified form of the high-level G3(MP2)-RAD procedure.[56] Modifications in the present study include the use of CCSD/6-31G(d,p) geometries and unscaled PBE/6-31G(d,p) zero-point vibrational energy corrections. For a small number of systems where we were unable to obtain CCSD/6-31G(d,p) geometries, the corresponding PBE/6-31G(d,p) geometry was used for the G3(MP2)-RAD calculation.

In all DMol^3 calculations, atom-centered grids were used for the numerical integration with the "Fine" option that includes about 2000 grid points for each atom and a real-space cutoff of 10.0 Å was imposed for numerical integration. Self-consistent-field (SCF) convergence criterion was set to the root-mean-square change in the electronic density to be less than 2.7×10^{-5} eV. The convergence criteria applied for geometry optimization were 2.7×10^{-4} eV for energy, 0.054 eV/Å for force, and 0.005 Å for displacement. The thermal occupation option in DMol^3, which uses a finite-temperature Fermi function to compute fractional occupations by mixing virtual orbitals into the occupied space, is often necessary to achieve SCF convergence in metallic systems. Therefore, we have performed the DMol^3 calculations both with Fermi occupations (PBE/DNP and PW91/DNP) and with the thermal occupation level set at 0.136 eV (BLYP/DNP(thermal), PBE/DNP(thermal), and PW91/DNP(thermal)). All energies determined in the present study have been corrected for zero-point vibrational energy. Aluminum and silicon atoms were calculated using the unrestricted nonsymmetrical formalism.

3. Results and Discussion

A. Assessment of $Al_{12}X$ Geometries. The Al_{13} and $Al_{12}Si$ clusters have been studied extensively by both theoretical and experimental procedures. However, in this study we wish to compare the performance of Delleys Double Numerical basis set with polarization (DNP)[50a] against analytical basis sets (6-31G(d,p) and 6-311G(d,p)) for the description of $Al_{12}X$ clusters and their interaction with hydrogen. Further to this we will also present results that compare the effect of the thermal occupation procedure versus the standard Fermi occupation. Table 1 presents calculated structural properties for Al_{13}, $Al_{12}Si$, and their respective monocations and monoanions, calculated with the PBE and PW91 functionals using the DNP, 6-31G(d,p), and 6-311G(d,p) basis sets, and at CCSD/6-31G(d,p), which provides a benchmark level for geometries in the absence of experimental data. For comparison, we also provide results for BLYP/DNP with thermal occupations, which we have used in a previous study,[46] and theoretical values from the literature [19−26,32,43,45] where available. Also included are mean absolute deviations (MADs), mean deviations (MDs), and largest deviations (LDs) from the CCSD/6-31G(d,p) level in the core−vertex bond lengths obtained with the DFT procedures.

As can be seen from the mean absolute deviations in Table 1, all levels give good overall performance for core−vertex distances compared to CCSD/6-31G(d,p). It is also clear that there is relatively little difference in the performance of the PBE and PW91 functionals with each of the respective basis sets. The PW91/6-311G(d,p) level performs best with a MAD of 0.003 Å, closely followed by the PBE/6-311G(d,p) and PBE/6-31G(d,p) levels. The PBE/DNP and PW91/DNP levels using Fermi occupations give performances almost identical to PW91/6-31G(d,p) and perform only slightly less well than PBE and PW91 with the larger 6-311G(d,p) basis set. Generally all of the procedures slightly underestimate the core−vertex distances obtained at CCSD/6-31G(d,p); however, our values are similar to those obtained in earlier studies.[19,21,23,26,32−34,36,37,39,43,45]

It can be seen from Table 1 that some methods give structures with different symmetries when the thermal occupation procedure is used. These methods also exhibit the largest MADs and LDs from CCSD/6-31G(d,p). Generally, these larger deviations occur for the open-shell systems and relate to the fact that *inclusion* of thermal occupations leads to fractional occupations of the HOMO, which in turn reduces the impact of Jahn−Teller distortions in several structures (Al_{13}^+, Al_{13}, $Al_{12}Si^+$, and $Al_{12}Si^-$). Consequently, this leads to a shortening of the "distorted" bond(s) and optimization to higher symmetry structures. The BLYP/DNP(thermal) procedure offers the poorest agreement with the CCSD/6-31G(d,p) level and is also the only procedure that systematically overestimates the core−vertex distances of these species.

B. Assessment of $Al_{12}X$ Energies. Table 2 presents energetic data for Al_{13} and $Al_{12}Si$ calculated at a range of DFT levels and compared with G3(MP2)-RAD as well as theoretical and experimental [5−11,13,41] values from the literature. The G3(MP2)-RAD level provides a benchmark for energies in this study and has previously[56] been found to give good overall performance for energies in the G2/97 test set. G3(MP2)-RAD essentially corresponds to the URCCSD(T)/G3MP2large//B3LYP/6-31G(d) + ZPVE energies, obtained using additivity approximations; however, we have modified the standard G3(MP2)-RAD procedure for this study to include CCSD/6-31G(d,p) geometries and unscaled PBE/6-31G(d,p) zero-point vibrational energies.[57]

With the exception of BLYP/DNP(thermal), there is generally very close agreement in the DFT binding energies (BEs) for Al_{13} and $Al_{12}Si$ species regardless of basis set or occupation scheme. In particular, our PBE and PW91 binding energies for Al_{13} are in excellent agreement with our benchmark G3(MP2)-RAD level, with deviations of −0.44 to +0.19 eV, while for $Al_{12}Si$ the deviations range from −0.80 to −0.30 eV. Excluding BLYP/DNP, all of our theoretical values for the binding energy of Al_{13} are higher (0.39−1.02 eV) than the experimental value of Ray et al.,[13] which may indicate that the experimental value is slightly low. The theoretical values of Calleja et al.[26] and Kumar et al.[37] using PBE with pseudopotential and PW91 with plane-wave basis sets, respectively, are slightly higher than our calculated values. However, the binding energies obtained by LDA methods are somewhat higher than our values, reflecting the known overbinding of these methods compared to GGA procedures.[32,33,35,36,38,43] There is only a relatively small basis set effect, with the 6-31G(d,p) values being 0.24 eV higher than the 6-311G(d,p) values while the DNP (Fermi) values are in fact only ∼0.11 eV higher than the 6-311G(d,p) values. However, binding energies at the BLYP/DNP level are generally 5−6 eV lower than the values obtained with PBE and PW91.

There have been relatively few studies of $Al_{12}X$ clusters at the CCSD level due to the computational expense, particularly for open-shell systems such as Al_{13}. In the study of Al_{13}^- by Dolgounitcheva at al.[29] single-point energies at the CCSD(T)/

TABLE 1: Structural Properties of $Al_{12}X$ (X = Al, Si,) Clusters (Å)

	BLYP/DNP (thermal)	PBE/DNP (thermal)	PBE/DNP	PBE/ 6-31G(d)	PBE/ 6-311G(d)	PW91/DNP (thermal)	PW91/DNP	PW91/ 6-31G(d)	PW91/ 6-311G(d)	CCSD/ 6-31G(d)	literature
						Al_{13}^+					
symm	I_h	I_h	C_1	C_2	C_2	I_h	C_1	C_2	C_2		
Al_c-Al_v	2.736	2.687	2.688−2.741	2.645−2.764	2.650−2.770	2.688	2.668−2.741	2.649−2.767	2.653−2.772		2.657−2.729[a]
Al_v-Al_v	2.877	2.826	2.676−2.942	2.686−2.954	2.690−2.959	2.826	2.676−2.942	2.734−2.986	2.736−2.960		
						Al_{13}					
symm	I_h	I_h	D_{3d}	D_{3d}	D_{3d}	I_h	D_{3d}	D_{3d}	D_{3d}	D_{3d}	
Al_c-Al_v	2.713	2.672[b]	2.655, 2.698	2.657, 2.705	2.660, 2.709	2.672	2.655,2.698	2.659, 2.707	2.662, 2.711	2.671, 2.711	2.68,[c] 2.70,[d] 2.78,[e] 2.60,[f] 2.72,[g] 2.752[h]
Al_v-Al_v	2.852	2.809[b]	2.748−2.961	2.752−2.961	2.759−2.962	2.809	2.748−2.961	2.757−2.962	2.757−2.967	2.754−2.980	2.815,[i] 2.85,[a] 2.86[g]
						Al_{13}^-					
symm	I_h	I_h	I_h	I_h	I_h	I_h	I_h	I_h	I_h	I_h	
Al_c-Al_v	2.700	2.663	2.663	2.667	2.671	2.664	2.663	2.669	2.672	2.673	2.652,[a] 2.752[i]
Al_v-Al_v	2.839	2.800	2.800	2.804	2.808	2.801	2.800	2.806	2.809	2.811	
						$Al_{12}Si^+$					
symm	D_{3d} (~I_h)	D_{3d} (~I_h)	D_{3d}	D_{3d}	D_{3d}	D_{3d} (~I_h)	D_{3d}	D_{3d}	D_{3d}	D_{3d}	
Si_c-Al_v	2.701, 2.702	2.650, 2.651	2.649, 2.672	2.655, 2.681	2.660, 2.687	2.653	2.650, 2.678	2.658, 2.684	2.662, 2.690	2.665, 2.689	
Al_v-Al_v	2.835−2.841	2.785, 2.788	2.732−2.944	2.740−2.944	2.744−2.951	2.789−2.791	2.735−2.939	2.741−2.950	2.744−2.959	2.745−2.957	
						$Al_{12}Si$					
symm	I_h	I_h	I_h	I_h	I_h	I_h	I_h	I_h	I_h	I_h	
$Si-Al_v$	2.682	2.642	2.642	2.651	2.651	2.642	2.642	2.649	2.653	2.651	2.76,[i] 2.67,[j] 2.64,[k] 2.66,[l] 2.59,[m] 2.64[n]
Al_v-Al_v	2.820	2.778	2.778	2.788	2.788	2.778	2.778	2.786	2.789	2.788	2.81,[j] 2.80,[l] 2.77[n]
						$Al_{12}Si^-$					
symm	I_h	I_h	D_{5d}	D_{5d}	D_{5d}	I_h	D_{5d}	D_{5d}	D_{5d}	D_{5d}	
$Si-Al_v$	2.696	2.653	2.620, 2.844	2.625, 2.851	2.628, 2.855	2.653	2.621, 2.844	2.627, 2.858	2.630, 2.860	2.627, 2.873	
Al_v-Al_v	2.835	2.790	2.741−2.855	2.746−2.862	2.749−2.865	2.790	2.741−2.855	2.748−2.866	2.750−2.868	2.747−2.872	
MD	+0.027	−0.016	−0.012	−0.006	−0.003	−0.015	−0.013	−0.013	−0.001		
MAD	0.039	0.025	0.012	0.006	0.003	0.024	0.013	0.013	0.003		
LD	−0.177	−0.222	−0.029	−0.022	−0.018	−0.217	−0.048	−0.102	−0.013		

[a] Duque.[45] [b] Goldberg and Yarovsky.[30] [c] Khanna.[43] [d] Khanna.[32] [e] Cheng.[21] [f] Yang.[23] [g] Calleja.[26] [h] Pettersson et al.[19] [i] Gong and Kumar.[33] [j] Kumar.[36] [k] Kumar et al.[37] [l] Charkin et al.[40] [m] Seitsonen et al.[34] [n] Sun et al.[38]

TABLE 2: Energetic (eV) Properties of $Al_{12}X$ (X = Al, Si) Clusters

	BLYP/DNP (thermal)	PBE/DNP (thermal)	PBE/DNP	PBE/ 6-311G(d)	PBE/ 6-311G(d)	PW91/DNP (thermal)	PW91/DNP	PW91/ 6-31G(d)	PW91/ 6-311G(d)	G3 (MP2)-RAD[a]	literature	expt
							Al_{13}					
state	^2A_g	^2A_g	$^2A_{2u}$	$^2A_{2u}$	$^2A_{2u}$	^2A_g	$^2A_{2u}$	$^2A_{2u}$	$^2A_{2u}$	$^2A_{2u}$		
binding energy (eV)	25.24	33.27	32.98	33.14	32.90	33.03	32.76	32.88	32.64	33.08	35.97,[b] 36.7;[c] 37.54,[d] 39.2;[e] 38.6;[f] 36.4;[g] 33.83,[h] 39.0;[i] 45.5;[j] 34.0[k]	32.25[l]
$E_{HOMO-LUMO}$ (eV)	1.80	1.99	1.75	1.75	1.78	1.98	1.74	1.75	1.75		1.57[h]	
IP (eV)	6.23	6.63	6.73	6.66	6.65	6.65	6.76	6.68	6.67	6.88[m]	7.10,[b] 7.2;[c] 6.8;[f] 6.0;[g] 7.15;[i] 6.92[n]	<6.42,[o] >6.4[p]
vDE (eV)											2.9;[g] 3.59;[q] 3.55[r]	3.75 ± 0.1,[s] 3.62[t]
EA (eV)	2.73		3.40	3.33	3.34		3.39	3.34	3.36	3.68	4.36,[b] 3.81[i]	2.86 ± 0.1,[u] 3.57 ± 0.05,[v] 2.6 ± 0.2,[w] 3.5[x]
							$Al_{12}Si$					
state	^1A_g	^1A_g	^1A_g	^1A_g	^1A_g	^1A_g	^1A_g	^1A_g	^1A_g			
binding energy (eV)	27.49	33.96	35.46	35.59	35.35	33.19	35.24	35.33	35.09	35.89	39.20,[b] 39.26,[c] 40.46,[d] 46.3;[f] 36.56,[h] 44.7;[y] 44.9[z]	
$E_{HOMO-LUMO}$ (eV)	1.21	2.04	2.04	2.02	2.03	2.03	2.02	2.01	2.01		1.99,[b] 2.75;[f] 1.99,[h] 1.90[aa]	
IP (eV)	6.06	6.46	6.73	6.72	6.71	6.48	6.74	6.72	6.72		6.5;[f] 6.78[r]	6.42–7.90[ab]
EA (eV)	1.86	2.09	1.85	1.80	1.83	2.10	1.88	1.83	1.86	1.96		1.69 ± 0.07[ab]

[a] CCSD/6-31G(d) geometry unless otherwise stated. [b] Gong and Kumar.[33] [c] Khanna.[43] [d] Kumar.[36] [e] Duque.[45] [f] Khanna.[32] [g] Cheng.[21] [h] Kumar et al.[37] [i] Yi.[20] [j] Yang.[23] [k] Calleja.[26] [l] Ray et al.[13] [m] Calculated using PBE/6-31G(d) geometry for Al_{13}^+. [n] Akola et al.[24] [o] Cox et al.[5] [p] Schriver et al.[6] [q] Akola et al.[25] [r] Charkin et al.[39] [s] Vertical IP, Cha et al.[9] [t] Li et al.[10] [u] Taylor et al.[8] [v] Li and Wang[11] [w] Ganteför et al.[7] [x] Burkart et al.[41] [y] Gong.[35] [z] Seitsonen et al.[34] [aa] Sun et al.[38] [ab] Akutsu et al.[59]

6-311G(d)//HF/3-21G(d) level were used to demonstrate that the icosahedral structure was lower in energy than the D_{5h} isomer. They also found that electron propagator predictions of the photoelectron spectrum of Al_{13}^- were in close agreement with experiment. Similarly, Han et al.[47] used single-point energies at the CCSD and CCSD(T) levels to compare the relative energies of various isomers of $Al_{13}H$. While Dolgounitcheva et al.[29] provide a total energy for Al_{13}^-, neither paper reports binding energies for the clusters studied. We find that the binding energies for Al_{13}, $Al_{12}Si$, and their cations and anions, at the frozen-core CCSD/6-31G(d) level, are significantly underestimated (e.g., BE for Al_{13} = 25.97 eV) relative to both the G3(MP2)-RAD level and the experimental value of Ray et al.[13] From single-point energies carried out on the CCSD/6-31G(d) geometry of Al_{13}, we find that increasing the basis set to 6-311G(d) has only a marginal effect (−0.2 eV). However, including perturbative contributions of connected triple excitations (T) in the calculation leads to a significant increase (3.65 eV) in the binding energy of Al_{13}, while increasing the correlation space to include the 2p electrons leads to a further increase (0.37 eV) in the binding energy to give a total value of 29.99 eV. Nevertheless, this value is still somewhat lower than the experimental value of 32.25 eV and the G3(MP2)-RAD value of 33.08 eV. Inclusion of core-correlation and relativistic effects as well as extrapolation to the infinite basis set limit should lead to further improvements; however, this is beyond the scope of this study. Clearly, description of the metallic bonding in these systems is quite a challenge for ab initio procedures, and it is fortunate that the less expensive DFT procedures perform so well. However, while the binding energies are underestimated at the CCSD(T)/6-31G(d) level, we find that IPs and EAs are in much closer agreement with experiment, suggesting that there is some cancellation of errors. We also note that the increased binding expected with the inclusion of triples excitations and correlation of the 2p electrons would be expected to lead to a shortening of the core−vertex distances in these clusters which may lead to even smaller MADs, MDs, and LDs for PBE/DNP and PW91/DNP.

In agreement with earlier studies,[32,33,35,38,43] our calculated binding energies for $Al_{12}Si$ are higher than the corresponding values for Al_{13}, reflecting the increased stability of the closed-shell configuration. Generally, our DFT binding energies for $Al_{12}Si$ are 2.19−2.48 eV greater than the corresponding values for Al_{13}, while our benchmark G3(MP2)-RAD level predicts an increase in binding energy of 2.81 eV. Earlier studies[32,33,35,36,38,43] predict somewhat greater increases in BE with silicon doping (∼2.6−7.7 eV), particularly those based on LDA procedures.

In addition to changes in binding energy, Kumar et al.[37] used the enthalpies of the following substitution reactions as a measure of the stability of $Al_{12}X$ (X = Si) relative to Al_{13}. An exothermic reaction indicates that the dopant X stabilizes the cluster, whereas an endothermic enthalpy indicates that X destabilizes the cluster.

$$Al_{13} + X \rightarrow Al_{12}X + Al \quad (1)$$

$$2Al_{13} + X_2 \rightarrow 2Al_{12}X + Al_2 \quad (2)$$

We obtain enthalpies of −2.19 to −2.80 eV for reaction 1 and −2.83 to −3.33 eV for reaction 2, with X = Si. In comparison, Kumar et al.[37] obtained values of −2.74 and −3.42 eV, respectively, at the PW91 level using ultrasoft pseudopotentials with plane-wave basis set. While our values are generally slightly smaller, both studies clearly indicate that substitution of the core aluminum atom with silicon leads to increased stability.

TABLE 3: Structural (Å) and Energetic (eV) Properties of $Al_{13}H$ Isomers

	PBE/DNP (thermal)	PBE/DNP	PBE/ 6-31G(d,p)	PBE/ 6-311G(d,p)	CCSD/ 6-31G(d,p)	literature
			$Al_{13}H$ (Atop)			
state	^1A	^1A	^1A	^1A		
H binding energy (eV)	2.21	2.49	2.51	2.47	2.48[a,b]	2.67,[c] 2.72,[d] 2.88,[e] 2.82,[f] 2.88,[g] 3.03,[h] 2.56,[i] 2.74,[j] 2.92,[k] 3.09[l]
$E_{HOMO-LUMO}$ (eV)	1.64	1.62	1.56	1.55		0.92,[d] 1.56,[f] 1.30,[g] 2.16,[h] 1.46,[i] 2.53[j]
symm	C_1	C_1	C_1	C_1		
Al_v-H (Å)	1.597	1.596	1.601	1.600		1.57,[c] 1.57,[d] 1.59[l]
Al_c-Al_{vH} (Å)	2.705	2.591	2.592	2.590		2.68,[c] 2.79[d]
			$Al_{13}H$ (Bridge)			
state	$^1A_1$	$^1A_1$	$^1A_1$	$^1A_1$	$^1A_1$	
H binding energy (eV)	2.40	2.68	2.71	2.67	2.68[a]	3.24,[b] 3.02,[d] 3.28,[e] 3.10,[f] 2.58,[g] 2.65,[h] 2.62,[i] 2.64[j]
$E_{HOMO-LUMO}$ (eV)	1.74	1.74	1.72	1.72		1.71,[d] 1.77,[f] 1.44,[g] 2.35,[h] 1.67,[i] 2.77[j]
symm	C_{2v}	C_{2v}	C_{2v}	C_{2v}	C_{2v}	
Al_v-H (Å)	1.800	1.800	1.805	1.801	1.767	1.76,[c] 1.79[d]
Al_c-Al_{vH} (Å)	2.617	2.617	2.620	2.624	2.627	2.68,[c] 2.80[d]
			$Al_{13}H$ (Hollow)			
state	$^1A_1$	$^1A_1$	$^1A_1$	$^1A_1$		
H binding energy (eV)	2.42	2.71	2.73	2.69	2.73[a]	3.01,[c] 3.36[e]
$E_{HOMO-LUMO}$ (eV)	1.91	1.90	1.88	1.88		1.86[d]
symm	C_{3v}	C_{3v}	C_{3v}	C_{3v}	C_{3v}	
Al_v-H (Å)	1.954	1.955	1.955	1.952	1.943	1.94,[d] 1.94[e]
Al_c-Al_{vH} (Å)	2.653	2.653	2.658	2.661	2.673	2.80,[d] 2.67[e]
			$Al_{12}SiH$ (Atop)			
state	$^2A'$	$^2A'$	$^2A'$	$^2A'$	$^2A'$	
H binding energy (eV)	1.77	1.75	1.78	1.75	1.60[a]	
$E_{HOMO-LUMO}$ (eV)	1.29	1.58	1.57	1.57		
symm	C_s	C_s	C_s	C_s	C_s	
Al_v-H (Å)	1.604	1.604	1.609	1.605	1.582	
Si_c-Al_{vH} (Å)	2.693	2.673	2.673	2.678	2.683	
			$Al_{12}SiH$ (Hollow)			
state	$^2A_2$	$^2A'$	$^2A'$	$^2A'$		
H binding energy (eV)	1.49	1.27	1.33	1.30	1.10[a,b]	
$E_{HOMO-LUMO}$ (eV)	1.58	0.47	0.50	0.51		
symm	C_{3v}	C_s	C_1	C_s		
Al_v-H (Å)	1.919	1.856, 1.979, 1.979	1.899, 1.900, 2.011	1.994, 1.901, 1.901		
Si_c-Al_{vH} (Å)	2.652	2.609, 2.609, 2.609	2.621, 2.621, 2.889	2.624, 2.624, 2.894		
			$Al_{13}H_2$ (Atop, Atop)			
state	$^2A_{1g}$	^2A_u	^2A_u	^2A_u	^2A_u	
H binding energy (eV)	2.37	2.38	2.42	2.37	2.44[a]	2.38[k]
$E_{HOMO-LUMO}$ (eV)	1.99	1.75	1.74	1.74		
symm	D_{5d}	C_i	C_i	C_i	C_i	
Al_v-H (Å)	1.594	1.594	1.597	1.596	1.576	
Si_c-Al_{vH} (Å)	2.653	2.645	2.646	2.651	2.649	
			$Al_{12}SiH_2$ (Atop, Atop)			
state	$^1A_{1g}$	$^1A_{1g}$	$^1A_{1g}$	$^1A_{1g}$	$^1A_{1g}$	
H binding energy (eV)	2.28	2.28	2.31	2.28	2.30	
$E_{HOMO-LUMO}$ (eV)	2.06	2.05	2.03	2.03		
symm	D_{5d}	D_{5d}	D_{5d}	D_{5d}	D_{5d}	
Al_v-H (Å)	1.594	1.593	1.596	1.594	1.575	
Si_c-Al_{vH} (Å)	2.628	2.626	2.630	2.635	2.627	
MAD	0.017	0.013	0.010	0.008		
MD	0.000	−0.007	−0.003	0.000		
LD	−0.034	−0.034	+0.038	+0.034		

[a] G3(MP2)-RAD energy. [b] PBE/6-31G(d) geometry. [c] Khanna and Jena.[43] [d] Kawamura.[44] [e] Duque et al.[45] [f] VWN/AVDZ from Han et al.[47] [g] BLYP/AVDZ from Han et al.[47] [h] B3LYP/AVDZ from Han et al.[47] [i] PBE/AVDZ from Han et al.[47] [j] PBE0/AVDZ from Han et al.[47] [k] Jung and Han.[48] [l] Charkin et al.[49]

There is essentially no basis set effect on the HOMO−LUMO gap using the PBE and PW91 functionals with Fermi occupations; however, the inclusion of thermal occupations leads to a slight increase (∼0.25 eV) in the gap compared to the corresponding Fermi values. This can again be related to the fact that the thermal occupation procedure effectively mixes some virtual orbitals into the occupied space, so that the resulting LUMO is generally higher in energy than for the case of Fermi occupation. Our calculated values for the HOMO−LUMO gap[58] of Al_{13} are somewhat larger than the PW91 value of Kumar et al.,[37] but all of the values support the previous findings that the Al_{13} cluster is quite stable. At both BLYP and PBE levels, the HOMO−LUMO gap of $Al_{12}Si$ is predicted to be slightly higher than that for Al_{13} and the values obtained are in close agreement with those of LSDA calculations of Gong[33] and the PW91 plane-wave ultrasoft pseudopotential results of Kumar and co-workers[37,38] while the SCF-LCAO-MO value predicted by Khanna et al.[32] is significantly larger.

Table 2 also presents ionization potentials (IPs) and electron affinities (EAs), compared with experimental and other theoretical[20,21,24,25,32,33,39,43] values where available. As for the binding energies there is very close agreement between the PBE and PW91 levels, while a partial cancellation of errors leads to a slightly improved performance by BLYP/DNP(thermal).

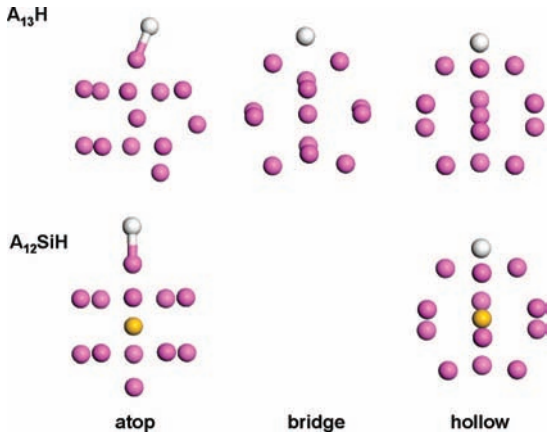

Figure 1. Isomers of $Al_{13}H$ and $Al_{12}SiH$.

We note that Cox et al.[5] suggest that the experimental IP of Al_{13} is slightly below 6.42 eV; however, Schriver et al.[6] interpret the IP for Al_{13} to actually be slightly greater than 6.4 eV. Our BLYP/DNP value is below 6.4 eV; however, the only other theoretical value below 6.4 eV that we are aware of is the LDA-DVM-Xα value of Cheng et al.[21] In comparison, our G3(MP2)-RAD, PBE, and PW91 values, calculated for the ^3B electronic state of Al_{13}^+, are all greater than 6.4 eV and in close agreement with the B3LYP theoretical value of Charkin et al.[39] Other theoretical values from the literature are generally higher than our results.[20,24,32,33,37,43]

Generally our calculated IPs for $Al_{12}Si$ ($Al_{12}Si^+$ in the $^2A_{2u}$ electronic state) are slightly higher than the corresponding values for Al_{13} and fall within the experimental range of Akutsu et al.[59] and are close to the theoretical value of Charkin et al.[39] However, for the procedures using thermal occupations, the IP of $Al_{12}Si$ is predicted to be lower (~0.2 eV) than that for Al_{13}. This can be related to the fact that the thermal occupations procedure generally has a larger effect in lowering the energy of open-shell species than that of closed-shell species. When thermal occupations are used, the energy of the system (A) is calculated as

$$A = U_{\text{thermal}} - TS$$

where U_{thermal} is the electronic energy with fractional occupations, T is the electronic energy, and S is the entropy; therefore, A is a free energy.[60] While U_{thermal} is greater than the electronic energy without fractional occupations ($U_{\text{nothermal}}$), the entropic contribution lowers A relative to $U_{\text{nothermal}}$.

The effect of thermal occupations on the IP of Al_{13} appears to be relatively small due to the fact that both Al_{13}^+ and Al_{13} are open-shell species and are lowered in energy to a similar extent. In comparison, while $Al_{12}Si^+$ is lowered in energy, the closed-shell $Al_{12}Si$ remains unchanged by the inclusion of thermal occupations and so the IP for this system is lowered.

Ganteför et al.[7] were able to obtain estimates of the vertical electron affinity[61] using photodetachment spectroscopy of cold cluster anions. They found that the first band of Al_{13}^- lies at an extraordinarily high energy. This result is in agreement with the jellium model which predicts shell closing for Al_{13}^- with 40 valence electrons. They also note that the adiabatic electron affinity (EA) can only be determined from these spectra if the vibrational structure of the electronic ground state is resolved and the 0−0 vibrational transition identified. However, recent interpretations[62] of photoelectron spectra assign the maximum of the photoelectron yield to the vertical detachment energy (vDE) while the onset threshold of the photoelectron yield is assigned to the adiabatic electron affinity. Clearly, if the structure of the neutral cluster and its anion are very similar, then the EA and vDE should also be very similar. However, if there is a significant difference in the structures, then there will also be a significant difference between the vDE and EA of the cluster. Table 1 indicates that there are slight differences in the structures of Al_{13} and Al_{13}^-; however, the experimental values of EA and vDE range from 2.6 to 3.75 eV. Only our BLYP/DNP electron affinity is in close agreement with the low-lying experimental value of Ganteför et al.,[7] while our PBE and PW91 values, calculated for the ^1A_g state of Al_{13}^-, are in closer agreement with the experimental value of Taylor et al.[8] However, the experimental value of Li and Wang[11] is significantly higher than all three of our theoretical values. Likewise, the experimental vDE value of Cha et al.[9] is significantly higher than our theoretical values.

Not surprisingly, the EA of $Al_{12}Si$ is significantly lower than that of the Al_{13}, reflecting the closed-shell nature of the $Al_{12}Si$ ($Al_{12}Si^-$ in the $^2A_{1g}$ electronic state). In $Al_{12}Si$ the extra electron has to go into the higher energy 1g jellium orbital; however, for Al_{13} the extra electron completes the 2p level, giving a stable closed-shell electronic configuration. There is generally very close agreement between all of the DFT levels for the EA of $Al_{12}Si$. However, thermal occupations has a significant effect on lowering the energy of $Al_{12}Si^-$, leading to an ~0.25 eV increase in the calculated EA values.

It is clear from Table 2 that the DNP numerical basis set generally gives comparable energies with the larger 6-311G(d,p) analytical basis set using both PBE and PW91, as well as offering good performance with respect to G3(MP2)-RAD and available experimental values. Therefore, we recommend the PBE/DNP level as a computationally cost-effective procedure for the investigation of aluminum clusters.

C. Assessment of $Al_{12}XH_n$ Geometries and Energies. Due to the similarity in the results obtained with PBE and PW91 for the $Al_{12}X$ clusters, we have limited our assessment of basis sets and occupations for the hydrogenated clusters to the PBE functional. Table 3 presents key data for the atop, bridge, and hollow isomers of $Al_{13}H$, the atop and hollow isomers of $Al_{12}SiH$, and the lowest energy isomers of $Al_{13}H_2$ and $Al_{12}SiH_2$, compared with available theoretical and experimental data from the literature. [43−49] Structures for the isomers of $Al_{13}H$ and $Al_{12}SiH$ are depicted in Figure 1.

As can be seen from Table 3, the PBE functional with each of our basis sets gives good agreement for the geometries of the $Al_{12}XH_n$ clusters compared with the benchmark CCSD/6-31G(d,p) level. The PBE/6-311G(d,p) level gives the smallest MAD, closely followed by PBE/6-31G(d,p). The MAD for PBE/DNP with Fermi occupations is slightly higher than that for PBE/6-31G(d,p) but is still quite acceptable, while that for PBE/DNP(thermal) is slightly higher again. Close inspection of Table 3 reveals that the DFT procedures tend to slightly overestimate the Al−H bond lengths and slightly underestimate the X_c-Al_v distances, relative to CCSD/6-31G(d,p). Likewise, our calculated Al−H bond lengths for $Al_{13}H$ are generally slightly longer than the literature values and our Al_c-Al_H distances for $Al_{13}H$ are generally shorter for all three isomers. There is only a relatively minor basis set effect on the geometries of the $Al_{12}XH_n$ clusters, which is demonstrated by a marginal increase in the X_c-Al_v distances for a small number of systems.

Open-shell structures again generally exhibit higher symmetry at the PBE/DNP(thermal) level than for the procedures using Fermi occupations. As discussed earlier, this is due to mixing of virtual orbitals into the occupied space, which lowers the

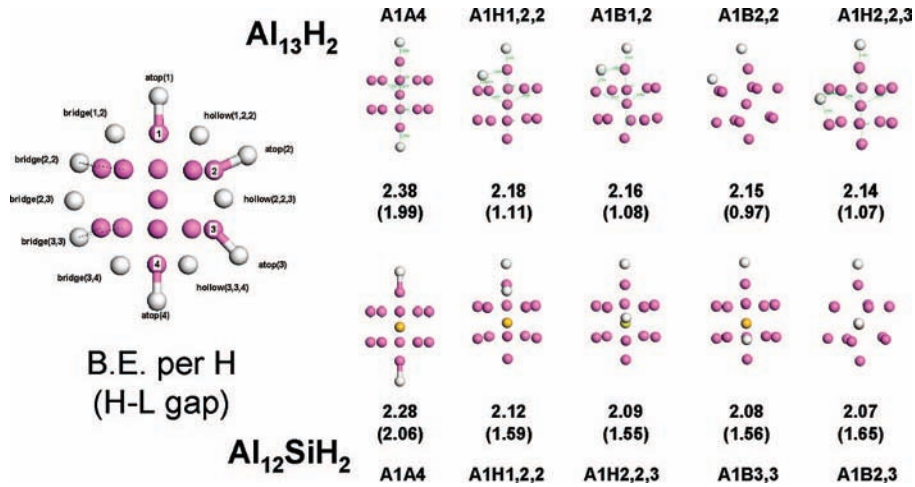

Figure 2. Low-energy isomers of $Al_{13}H_2$and $Al_{12}SiH_2$at PBE/DNP level.

effects of Jahn−Teller distortions. Consequently, the HOMO−LUMO gaps for the open-shell hydrogenated systems at PBE/DNP(thermal) are generally different from that of the corresponding Fermi optimized systems. For $Al_{12}SiH$ (hollow) and $Al_{13}H_2$ there is an ~0.25 increase in the calculated HOMO−LUMO gap, however, for $Al_{12}SiH$ (atop) thermal occupations leads to an ~0.3 eV decrease in the HOMO−LUMO gap.

The preferred location of hydrogen adsorption on the Al_{13} cluster has involved some debate and seems to depend greatly on the level of theory used, with the bridge and/or hollow sites generally considered the preferred locations.[43−49] However, early theoretical studies of $Al_{13}H$ isomers appear to have only considered structures in which the Al_{13} cluster was constrained to icosahedral symmetry or showed minimal distortion of the cluster. Khanna and Jena[53] note that Al_{13} reacts strongly with hydrogen and found, using DFT calculations within the local density approximation (LDA), that the binding energy for hydrogen in the bridge site of $Al_{13}H$ was greater than that for the atop position. However, Mañanes et al.[45] found using the local spin density approximation (LSDA) that the atop and bridge structures were saddle points and that the lowest energy structure had the hydrogen in a hollow position. The generalized gradient approximation (GGA) calculations of Kawamura et al.[44] (PW91/plane-wave pseudopotentials) indicated that the bridge and hollow structures for $Al_{13}H$ are very close in energy. However, as we reported previously,[46] the lowest energy isomer for $Al_{13}H$ at the BLYP/DNP level is a significantly distorted Al_{13} cluster (root-mean-square deviation from I_h symmetry is 0.421) with the H atom in an atop position and the binding energy of H to the cluster being 2.88 eV. Han et al.[47] also found the distorted atop position to be lowest in energy at the BLYP/aug-cc-pVDZ level, with a hydrogen binding energy also of 2.88 eV. Both studies find binding to the bridge and hollow sites to be ~0.2 eV lower than the atop position. The B3LYP study of Charkin et al.[49] also identified distorted isomers of $Al_{13}H$ lower in energy than the more symmetric structures and found the distorted atop structure to be lowest in energy.

In the present study with PBE, all levels predict that the bridge and hollow isomers of $Al_{13}H$ are the most stable and are almost degenerate in energy, while the atop isomer is found to be slightly higher in energy. Our results are in agreement with the PBE/aug-cc-pVDZ results of Han et al.,[47] who report a binding energy for hydrogen in the hollow, bridge, and atop sites of 2.64, 2.62, and 2.48 eV, respectively, compared with our values of 2.73, 2.71, and 2.5 eV, respectively, at the PBE/6-31G(d,p) level. We also note that the PBE levels with Fermi occupations give excellent agreement with the benchmark G3(MP2)-RAD level for the binding energy of H in $Al_{13}H$ isomers. Generally, the literature values using LDA (VWN and SVWN) give greater binding energies for hydrogen to Al_{13} than our PBE and G3(MP2)-RAD procedures. Reinforcing the predicted stability of $Al_{13}H$ (hollow), all PBE levels predict that the HOMO−LUMO gap for the hollow isomer is the largest, with the atop the lowest. However, the values for all three isomers are higher than the experimental estimate (~1.4 eV) of Burkart et al.[41]

As for $Al_{13}H$, addition of hydrogen atom to $Al_{12}Si$ is found to proceed without a barrier. However, for $Al_{12}SiH$, the atop isomer is found to be lowest in energy and the cluster exhibits very little structural distortion. Likewise, there is relatively little distortion from C_{3v} symmetry for the higher energy hollow structure. We were unable to locate local minima corresponding to the bridge structure of $Al_{12}SiH$. The calculated Al−H bond length for the atop isomer of $Al_{12}SiH$ is found to be marginally longer than Al−H in $Al_{13}H$ (atop) at all levels investigated, while for the hollow isomer, the Al−H distances are generally slightly shorter than the corresponding values in $Al_{13}H$ (hollow).

Similarly, the hydrogen binding energies for $Al_{12}SiH$ are substantially lower than the corresponding values for $Al_{13}H$. This difference in binding energy reflects the fact that $Al_{12}Si$ already has a completed valence electronic shell and therefore has less affinity for hydrogen atom compared to Al_{13}, where the single electron of the H atom completes the valence shell of the cluster. The HOMO−LUMO gaps for the atop and hollow isomers of $Al_{12}Si$ are lower than the corresponding values for Al_{13}.

There is essentially no basis set effect on the binding energies of hydrogen in the selected $Al_{12}XH_n$ clusters, with DNP performing equally well as the larger and more expensive 6-311G(d,p) basis set. However, inclusion of thermal occupations does appear to have an effect on the binding energies of several systems involving open-shell species. For example, the binding energies for hydrogen in the isomers of $Al_{13}H$ are ~0.3 eV lower using the PBE/DNP(thermal) level compared to PBE/DNP(Fermi) due to the energy lowering effect on the open-shell Al_{13} cluster. Thermal occupations also lowers the energy of $Al_{12}SiH$ (hollow), resulting in an increase in the binding energy for hydrogen relative to the corresponding Fermi calculation. In the case of $Al_{13}H_2$ where the two open-shell species ($Al_{13}H_2$ and Al_{13}) are lowered in energy to a similar extent, there is a cancellation of the effect.

D. $Al_{12}XH_2$ Isomers. Screening of structural isomers of $Al_{12}XH_2$ (X = Al, Si) was carried out at the PBE/DNP level,

and the five lowest energy structures are shown in Figure 2, with the binding energy per hydrogen and HOMO−LUMO gap (in parentheses) and with a schematic of the nomenclature used to describe each adsorption site. Assessment of effects due to basis set and electronic occupation scheme was only performed on the lowest energy isomer of $Al_{13}H_2$ and $Al_{12}SiH_2$ (Table 3).

As indicated in Table 3 and Figure 2, the lowest energy structure for $Al_{13}H_2$ has the hydrogen atoms in opposing atop positions (atop(1)−atop(4)). The calculated binding energies per hydrogen atom are only slightly less than that for a single hydrogen in the atop position of $Al_{13}H$, using Fermi occupations. The fact that the binding energy of the second hydrogen is less than that of the first (−0.1 eV) is not surprising given that the first hydrogen enables the cluster to achieve a closed 2p valence electronic shell, whereas the second hydrogen leads to an open-shell electronic structure. However, we might have expected a larger decrease for the second hydrogen, given that H binding to $Al_{12}Si$, which is isoelectronic with $Al_{13}H$, is significantly lower. Jun and Han[48] also identified the atop(1)−atop(4) structure as the lowest energy isomer of $Al_{13}H_2$. Their binding energy for the second hydrogen atom (2.38 eV) at the PBE0/6-311G(d,p) level agrees closely with our values. The Al−H bond lengths for this structure are essentially the same as the Al−H distance in $Al_{13}H$ (atop). However, the axial Al_c-Al_v distance (∼2.65 Å) is slightly longer than the value in the distorted atop Al_{13} isomer but still slightly less than in the bare Al_{13} structure. The remaining Al−Al distances are 2.643−2.701 Å, which is essentially the same as in the bare cluster. The HOMO−LUMO gap for this highly symmetric structure is similar to that for the bare cluster and significantly larger than for the remaining structural isomers of $Al_{13}H_2$.

The next four low energy isomers of $Al_{13}H_2$ have the two hydrogen atoms bound to adjacent surface aluminum atoms with one hydrogen in an atop position and the second in a bridge or hollow position. The binding energy of the hydrogens to the atop(1)−hollow(1,2,2) isomer is slightly greater than for the other structures, which are almost degenerate in energy. The HOMO−LUMO gap for the atop(1)−hollow(1,2,2) isomer is also slightly larger than for the other isomers. The fifth lowest energy isomer is closely related to the atop(1)−bridge(2,2) isomer but has the second hydrogen located in a central hollow rather than a bridge position. In the subsequent structures there is a further gradual decline in the binding energy of the hydrogen to the cluster. Generally for these systems one hydrogen is located in an atop position with the second located progressively in hollow, bridge, and then atop positions.

Figure 2 also presents a selection of the lowest energy $Al_{12}SiH_2$ structural isomers. As for $Al_{13}H_2$, the lowest energy isomer of $Al_{12}SiH_2$ has the two hydrogen atoms in atop positions on opposing sides of the cluster (atop(1)−atop(4)) with almost no distortion of the symmetry of the underlying cluster. Surprisingly, all levels predict that the binding energy for hydrogen in this isomer is greater than the binding energy of hydrogen atom in $Al_{12}SiH$ (atop). In conjunction with this, the Al−H distances in this structure are slightly shorter than the Al−H distance in $Al_{12}SiH$. Less surprisingly, the BE of hydrogen in the $Al_{12}SiH_2$ cluster is less than for the corresponding isomer of $Al_{13}H_2$. The HOMO−LUMO gap for $Al_{12}SiH_2$ atop(1)−atop(4) is also significantly greater than for the atop and hollow isomers of $Al_{12}SiH$.

The hydrogen binding energies for the remaining isomers of $Al_{12}SiH_2$ are lower (0.1 eV per hydrogen) than for the atop(1)−atop(4) structure, but as can be seen from Figure 2 the hydrogen BE remains greater than twice that of one hydrogen in the atop isomer of $Al_{12}SiH$. However, there is a substantial drop in the HOMO−LUMO gap for these isomers. For these isomers the second hydrogen adopts hollow and bridge sites in preference to atop positions. We note that, in a small number of examples at the BLYP/DNP level, geometry optimization of $Al_{12}SiH_2$ leads to a distorted structure that more closely resembles a decahedral rather than an icosahedral structure.

As noted for $Al_{12}XH$ systems, there is essentially no basis set effect for the geometries and energies of $Al_{12}XH_2$ (X = Al, Si) systems (Table 3). Further to this, the PBE level with Fermi occupation generally gives good agreement with CCSD/6-311G(d,p) for geometries and G3(MP2)-RAD for binding energies. Thermal occupations again lead to energy lowering and increase in the HOMO−LUMO gap of the open-shell species, relative to Fermi occupations.

4. Conclusions

We have investigated and compared the ability of numerical and Gaussian-type basis sets combined with density functional theory to accurately describe the geometries, binding energies, and electronic properties of aluminum clusters, $Al_{12}XH_n$ (X = Al, Si; n = 0, 1, 2). Generally, the PBE functional with the double numerical basis set with polarization (DNP) performs very well against the analytical basis sets for considerably less computational expense. Our study indicates that the PBE/DNP level generally gives results comparable to those of the CCSD/6-31G(d,p) level for $Al_{12}XH_n$ cluster geometries with a mean absolute deviation for bond lengths only slightly greater than observed with PBE/6-31G(d,p) and PBE/6-311G(d,p). The PBE/DNP level also performs well for assessment of cluster binding energies, ionization potentials, and electron affinities compared with experiment and the high-level G3(MP2)-RAD procedure. Therefore, we recommend the PBE/DNP level as a computationally cost-effective procedure for the investigation of aluminum clusters.

The thermal occupations procedure, which uses a finite temperature Fermi function to compute fractional occupations by mixing virtual orbitals into the occupied space, generally affects the structures and energies of open-shell systems to a greater extent than closed-shell species. Consequently, the open-shell species generally exhibit higher symmetry when calculated with thermal occupations and have slightly larger MADs for bond lengths, compared to systems calculated with standard Fermi occupations. Thermal occupations also generally leads to a more significant lowering of the energy of open-shell species than of closed-shell species, which has an impact on binding energies, ionization potentials, and electron affinities involving these species. Similarly, since the procedure involves mixing of virtual orbitals into the occupied space, the magnitude of the HOMO−LUMO gap for these species is generally larger compared to the corresponding Fermi calculated value.

Our calculations also show that hydrogen binds to the $Al_{12}X$ clusters (X = Al, Si) without a barrier and that the binding of hydrogen atom to Al_{13} is quite strong while the binding to the closed-shell $Al_{12}Si$ cluster is substantially weaker. In the case of Al_{13}, the preferred location of the hydrogen appears to depend on the DFT procedure used, with the hollow site marginally favored over the bridge site at PBE/DNP. For the $Al_{12}Si$ cluster the atop position is favored with little distortion of the underlying cluster symmetry.

A large number of structural isomers of $Al_{12}XH_2$ (X = Al, Si) were investigated, and the lowest energy isomers were found to be those in which the hydrogen atoms are in atop positions

on opposite sides of the cluster. The binding energy for the two hydrogen atoms in $Al_{13}H_2$ is slightly less than double the binding energy for a single hydrogen in the atop position. Surprisingly, the binding energy for the two hydrogen atoms to the closed-shell $Al_{12}Si$ is significantly more than twice the binding energy of one hydrogen atom to $Al_{12}Si$.

There is essentially no basis set effect for the geometries and energies of $Al_{12}XH_n$ (X = Al, Si; $n = 1, 2$) systems at the PBE level. Further to this, the PBE level with Fermi occupation generally gives good agreement with CCSD/6-311G(d,p) for geometries and G3(MP2)-RAD for binding energies. Thermal occupations generally leads to energy lowering and increase in the HOMO−LUMO gap of the open-shell species, relative to Fermi occupations.

Acknowledgment. We gratefully acknowledge the award of an Australian Research Council Discovery Grant to carry out this work. We also gratefully acknowledge allocation of computing time from the National Facility of the Australian Partnership for Advanced Computing (APAC). We would also like to thank Dr. Bernard Delley and Dr. Alexander Goldberg for helpful discussions.

References and Notes

(1) *Metal Clusters*; Moskovits, M. Ed.; Wiley and Sons: New York, 1986.

(2) *Clusters of Atoms and Molecules: Theory, Experiment and Clusters of Atoms*; Haberland, H. Ed.; Springer Series in Chemical Physics 52; Springer-Verlag: New York, 1995.

(3) *Clusters and Nanomaterials*; Kawazoe, Y., Ohno, K., Kondow, T. Eds.; Springer: New York, 2002.

(4) *Clusters and Nano-Assemblies*: Jena, P., Khanna, S. N., Rao, B. K. Eds.; World Scientific: Singapore, 2005.

(5) Cox, D. M.; Trevor, D. J.; Whetten, R. L.; Kaldor, A. *J. Phys. Chem.* **1988**, *92*, 421–429.

(6) Schriver, K.; Persson, J. L.; Honea, E. C.; Whetten, R. L. *Phys. Rev. Lett.* **1990**, *64*, 2539–2542.

(7) Ganteför, G.; Meiwes-Broer, K. H.; Lutz, H. O. *Phys. Rev. A* **1988**, *37*, 2716–2718.

(8) Taylor, K. J.; Pettiette, C. L.; Craycraft, M. J.; Chesnovsky, O.; Smalley, R. E. *Chem. Phys. Lett.* **1988**, *152*, 347–352.

(9) (a) Cha, C.-Y.; Ganteför, G.; Eberhardt, W. *J. Chem. Phys.* **1994**, *100*, 995–1010. (b) Ganteför, G.; Eberhardt, W. *Chem. Phys. Lett.* **1994**, *217*, 600–604.

(10) Li, X.; Wu, H.; Wang, X.-B.; Wang, L.-S. *Phys. Rev. Lett.* **1998**, *81*, 1909–1912.

(11) Li, X.; Wang, L.-S. *Phys. Rev. B* **2002**, *65*, 153404.

(12) De Heer, W. A.; Milani, P.; Châtelain, A. *Phys. Rev. Lett.* **1989**, *63*, 2834–2936.

(13) (a) Jarrold, M. F.; Bower, J. E.; Kraus, J. S. *J. Chem. Phys.* **1987**, *86*, 3876–3885. (b) Jarrold, M. F.; Bower, J. E. *J. Chem. Phys.* **1987**, *87*, 1610–1619. (c) Ray, U.; Jarrold, M. F.; Bower, J. E.; Kraus, J. S. *J. Chem. Phys.* **1989**, *91*, 2912–2921.

(14) King, F. L.; Ross, M. M. *Chem. Phys. Lett.* **1989**, *164*, 131–136.

(15) Cottancin, E.; Pellarin, M.; Lermé, J.; Baguenard, B.; Palpant, B.; Vialle, J. L.; Broyer, M. *J. Chem. Phys.* **1997**, *107*, 757–770.

(16) (a) Jarrold, M. F.; Bower, J. E. *J. Chem. Phys.* **1986**, *85*, 5373–5375. (b) Jarrold, M. F.; Bower, J. E. *J. Chem. Phys.* **1987**, *87*, 5728–5738. (c) Jarrold, M. F.; Bower, J. E. *Chem. Phys. Lett.* **1988**, *144*, 311–316. (d) Jarrold, M. F.; Bower, J. E. *J. Am. Chem. Soc.* **1988**, *110*, 70–78.

(17) (a) Leuchtner, R. E.; Harms, A. C.; Castleman, A. W. *J. Chem. Phys.* **1989**, *91*, 2753–2754. (b) Leuchtner, R. E.; Harms, A. C.; Castleman, A. W. *J. Chem. Phys.* **1991**, *94*, 1093–1101.

(18) McHenry, M. E.; Eberhart, M. E.; O'Handley, R. C.; Johnson, K. H. *Phys. Rev. Lett.* **1986**, *56*, 81–84.

(19) (a) Bauschlicher, C. W.; Pettersson, L. G. M. *J. Chem. Phys.* **1986**, *84*, 2226–2232. (b) Pettersson, L. G. M.; Bauschlicher, C. W.; Halicioglu, T. *J. Chem. Phys.* **1987**, *87*, 2205–2213.

(20) (a) Yi, J.-Y.; Oh, D. J.; Bernholc, J.; Car, R. *Chem. Phys. Lett.* **1990**, *174*, 461–466. (b) Yi, J.-Y.; Oh, D. J.; Bernholc, J. *Phys. Rev. Lett.* **1991**, *67*, 1594–1597.

(21) Cheng, H.-P.; Berry, R. S.; Whetten, R. L. *Phys. Rev. B* **1991**, *43*, 10647–10653.

(22) Rothlisberger, U.; Andreoni, W.; Giannozzi, P. J. *Chem. Phys.* **1992**, *96*, 1248–1256.

(23) Yang, S. H.; Drabold, D. A.; Adams, J. B.; Sachdev, A. *Phys. Rev. B* **1993**, *47*, 1567–1576.

(24) Akola, J.; Häkkinen, H.; Manninen, M. *Phys. Rev. B* **1998**, *58*, 3601–3604.

(25) Akola, J.; Manninen, M.; Häkkinen, H.; Landman, U.; Li, X.; Wang, L.-S. *Phys. Rev. B* **1999**, *60*, 11297–11300.

(26) Calleja, M.; Rey, C.; Alemany, M. M. G.; Gallego, L. J.; Ordejón, P.; Sánchez-Portal, D.; Artacho, E.; Soler, J. M. *Phys. Rev. B* **1999**, *60*, 2020–2024.

(27) Rao, B. K.; Jena, P. *J. Chem. Phys.* **1999**, *111*, 1890–1904.

(28) Ahlrichs, R.; Elliot, S. D. *Phys. Chem. Chem. Phys.* **1999**, *1*, 13–21.

(29) Dolgounitcheva, O.; Zakrzewski, V. G.; Ortiz, J. V. *J. Chem. Phys.* **1999**, *111*, 10762–10765.

(30) Goldberg, A.; Yarovsky, I. *Phys. Rev. B* **2007**, *75*, 195403.

(31) (a) Knight, W. D.; Clemenger, K.; de Heer, W. A.; Saunders, W. A.; Chou, M. Y.; Cohen, M. L. *Phys. Rev. Lett.* **1984**, *52*, 2141–2143. (b) Beck, D. E. *Solid State Commun.* **1984**, *49*, 381–385. (c) Chou, M. Y.; Cohen, M. L. *Phys. Lett.* **1986**, *113A*, 420–424.

(32) (a) Khanna, S. N.; Jena, P. *Phys. Rev. Lett.* **1992**, *69*, 1664–1667. (b) Khanna, S. N.; Jena, P. *Phys. Rev. Lett.* **1993**, *71*, 208.

(33) Gong, X. G.; Kumar, V. *Phys. Rev. Lett.* **1993**, *70*, 2078–2081.

(34) (a) Sietsonen, A. P.; Puska, M. J.; Alatalo, M.; Nieminen, R. M.; Milman, V.; Payne, M. C. *Phys. Rev. B* **1993**, *48*, 1981–1983. (b) Seitsonen, A. P.; Laasonen, L.; Nieminen, R. M.; Klein, M. L. *J. Chem. Phys.* **1995**, *103*, 8075–8080.

(35) Gong, X. G. *Phys. Rev. B* **1997**, *56*, 1091–1094.

(36) Kumar, V.; Sundararajan, V. *Phys. Rev. B* **1998**, *57*, 4939–4942.

(37) Kumar, V.; Bhattacharjee, S.; Kawazoe, Y. *Phys. Rev. B* **2000**, *61*, 8541–8547.

(38) Sun, Q.; Wang, Q.; Yu, J. Z.; Kumar, V.; Kawazoe, Y. *Phys. Rev. B* **2001**, *63*, 193408.

(39) Xie, R.-H.; Bryant, G. W.; Zhao, J.; Kar, T.; Smith, V. H. *Phys. Rev. B* **2005**, *71*, 125422.

(40) (a) Charkin, O. P.; Charkin, D. O.; Klimenko, N. M.; Mebel, A. M. *Chem. Phys. Lett.* **2002**, *365*, 494–504. (b) Charkin, O. P.; Klimenko, N. M.; Charkin, D. O.; Mebel, A. M. *Russ. J. Inorg. Chem.* **2004**, *49*, 1382–1391. (c) Charkin, O. P.; Klimenko, N. M.; Charkin, D. O.; Mebel, A. M. *Russ. J. Inorg. Chem.* **2004**, *49*, 1898–1905. (d) Charkin, O. P.; Klimenko, N. M.; Charkin, D. O.; Mebel, A. M. *Russ. J. Inorg. Chem.* **2005**, *50*, S17–S40.

(41) Burkart, S.; Blessing, N.; Klipp, B.; Müller, J.; Ganteför, G.; Seifert, G. *Chem. Phys. Lett.* **1999**, *301*, 546–550.

(42) Partridge, H.; Bauschlicher, C. W. *J. Chem. Phys.* **1986**, *84*, 6507–6510.

(43) (a) Khanna, S. N.; Jena, P. *Chem. Phys. Lett.* **1994**, *218*, 383–386. (b) Khanna, S. N.; Jena, P. *Phys. Rev. B* **1995**, *51*, 13705–13716.

(44) Kawamura, H.; Kumar, V.; Sun, Q.; Kawazoe, Y. *Phys. Rev. B* **2001**, *65*, 045406.

(45) (a) Duque, F.; Molina, L. M.; López, M. J.; Mañanes, A.; Alonso, J. A. *Eur. Phys. J. D* **2001**, *16*, 285–288. (b) Duque, F.; Mañanes, A.; Molina, L. M.; López, M. J.; Alonso, J. A. *Int. J. Quantum Chem.* **2002**, *86*, 226–238. (c) Alonso, J. A.; López, M. J.; Molina, L. M.; Duque, F.; Mañanes, A. *Nanotechnology* **2002**, *13*, 253–257. (d) Mañanes, A.; Duque, F.; Méndez, F.; López, M. J.; Alonso, J. A. *J. Chem. Phys.* **2003**, *119*, 5128–5141.

(46) Yarovsky, I.; Goldberg, A. *Mol. Simul.* **2005**, *31*, 475–481.

(47) Han, Y.-K.; Jung, J.; Kim, K. H. *J. Chem. Phys.* **2005**, *122*, 124319.

(48) Jung, J.; Han, Y.-K. *J. Chem. Phys.* **2006**, *125*, 064306.

(49) Charkin, O. P.; Kochnev, V. K.; Klimenko, N. M. *Russ. J. Inorg. Chem.* **2006**, *51*, 1925.

(50) (a) Delley, B. *J. Chem. Phys.* **1990**, *92*, 508–517. (b) Delly, B. In *Density Functional Theory: A Tool for Chemistry*; Seminario, J. M.,; Politzer, P. Eds.; Elsevier: Amsterdam, The Netherlands, 1995. (c) Delley, B. *J. Chem. Phys.* **2000**, *113*, 7756–7764.

(51) Frisch, M. J.; Trucks, G. W.; Schlegel, H. B.; Scuseria, G. E.; Robb, M. A.; Cheeseman, J. R.; Montgomery, J. A., Jr.; Vreven, T.; Kudin, K. N.; Burant, J. C.; Millam, J. M.; Iyengar, S. S.; Tomasi, J.; Barone, V.; Mennucci, B.; Cossi, M.; Scalmani, G.; Rega, N.; Petersson, G. A.; Nakatsuji, H.; Hada, M.; Ehara, M.; Toyota, K.; Fukuda, R.; Hasegawa, J.; Ishida, M.; Nakajima, T.; Honda, Y.; Kitao, O.; Nakai, H.; Klene, M.; Li, X.; Knox, J. E.; Hratchian, H. P.; Cross, J. B.; Bakken, V.; Adamo, C.; Jaramillo, J.; Gomperts, R.; Stratmann, R. E.; Yazyev, O.; Austin, A. J.; Cammi, R.; Pomelli, C.; Ochterski, J. W.; Ayala, P. Y.; Morokuma, K.; Voth, G. A.; Salvador, P.; Dannenberg, J. J.; Zakrzewski, V. G.; Dapprich, S.; Daniels, A. D.; Strain, M. C.; Farkas, O.; Malick, D. K.; Rabuck, A. D.; Raghavachari, K.; Foresman, J. B.; Ortiz, J. V.; Cui, Q.; Baboul, A. G.; Clifford, S.; Cioslowski, J.; Stefanov, B. B.; Liu, G.; Liashenko, A.; Piskorz, P.; Komaromi, I.; Martin, R. L.; Fox, D. J.; Keith, T.; Al-Laham, M. A.; Peng, C. Y.; Nanayakkara, A.; Challacombe, M.; Gill, P. M. W.; Johnson, B.; Chen, W.; Wong, M. W.; Gonzalez, C.; Pople, J. A. *Gaussian 03*, revision D.01; Gaussian, Inc.: Wallingford, CT, 2004.

(52) Werner, H.-J.; Knowles, P. J.; Lindh, R.; Schütz, M.; Celani, P.; Korona, T.; Manby, F. R.; Rauhut, G.; Amos, R. D.; Bernhardsson, A.; Berning, A.; Cooper, D. L.; Deegan, M. J. O.; Dobbyn, A. J.; Eckert, F.; Hampel, C.; Hetzer, G.; Lloyd, A. W.; McNicholas, S. J.; Meyer, W.; Mura, M. E.; Nicklass, A.; Palmieri, P.; Pitzer, R. ; Schumann, U.; Stoll, H.;. Stone, A. J.; Tarroni, R.; Thorsteinsson, T. *MOLPRO*, version 2006.1; see http://www.molpro.net.

(53) Perdew, J. P.; Burke, K.; Ernzerhof, M. *Phys. Rev. Lett.* **1996**, *77*, 3865–3868.

(54) Perdew, J. P.; Wang, Y. *Phys. Rev. B* **1996**, *45*, 13244–13249.

(55) Fowler, J. E.; Ugalde, J. M. *Phys. Rev. A* **1998**, *58*, 383–388.

(56) Henry, D. J.; Sullivan, M. B.; Radom, L. *J. Chem. Phys.* **2003**, *118*, 4849–4860.

(57) In a small number of systems where we were unable to obtain CCSD/6-31G(d,p) geometries, we have used the PBE/6-31G(d,p) geometry as an alternative.

(58) Since Al_{13} is an open-shell structure, our calculated HOMO−LUMO gaps are strictly the difference in energy of the singly occupied orbital (SOMO) and the LUMO, i.e., the difference in energy of the SOMO and the lowest energy virtual α-orbital. Some authors have reported much lower values for the HOMO−LUMO gap of Al_{13} which appear to correspond to the energy difference between the SOMO and the lowest energy virtual β-orbital.

(59) Akutsu, M.; Koyasu, K.; Atobe, J.; Hosoya, N.; Miyajima, K.; Mitsui, M.; Nakajima, A. *J. Phys. Chem. A* **2006**, *110*, 12073–12076.

(60) Weinert, M.; Davenport, J. W. *Phys. Rev. B* **1992**, *45*, 13709–13712.

(61) The adiabatic electron affinity is the energy difference between the ground states of the anion and the neutral, while the vertical electron affinity is the energy difference between the anion and neutral in the neutral geometry. Alternatively, the vertical detachment energy of an anion is the difference in energy between the ground state of the anion and the energy of the neutral having the anionic geometry.

(62) See, for example, the discussion in: Desfrançois, C.; Schermann, J. P. *Chem. Soc. Rev.* **2002**, *31*, 269–274.

JP802389B